J. Braz. Chem. Soc., Vol. 23, No. 1, 32-38, 2012.
Printed in Brazil - ©2012 Sociedade Brasileira de Química
0103 - 5053 $6.00+0.00

Article

Pt $L_{2,3}$ - Edge X-ray Absorption Spectroscopy Investigation of Zerovalent $[Pt(PPh_3)_2(\eta^2\text{-}L)]$ {L = C_2H_4, C_{60} and $C_2(CN)_4$} Compounds

Gilson H. M. Dias,[a] Nazareth F. da Fonseca[b] and Marcelo H. Herbst*[*,b]

[a]*Instituto de Química, Universidade Estadual de Campinas, CP 6154, 13083-970 Campinas-SP, Brazil*

[b]*Departamento de Química, Universidade Federal Rural do Rio de Janeiro, 23890-000 Seropédica-RJ, Brazil*

Espectros de absorção de raios X nas bordas $L_{2,3}$ da platina (Pt) de três compostos $[Pt(PPh_3)_2(\eta^2\text{-}L)]$ {L = C_2H_4, C_{60} and $C_2(CN)_4$} foram obtidos. As bandas de absorção observadas são efetivas para mensurar a força π^*-ácida dos ligantes olefínicos (L) coordenados ao fragmento $Pt(PPh_3)_2$. As energias dos orbitais d_π, determinadas quantitativamente pela diferença entre os deslocamentos das inflexões das bordas e de seus máximos nas linhas brancas $L_{2,3}$ nas segundas derivadas dos espectros, seguem a ordem $[Pt(PPh_3)_2(\eta^2\text{-}C_2H_4)] < [Pt(PPh_3)_2(\eta^2\text{-}C_{60})] < [Pt(PPh_3)_2\{\eta^2\text{-}C_2(CN)_4\}]$. Essas energias dos orbitais d_π estão em concordância com as alterações nos comprimentos de ligação das olefinas livres e coordenadas, e com os deslocamentos químicos de coordenação no espectro de RMN de ^{31}P dos compostos. Além disso, os valores experimentais concordam com resultados teóricos obtidos para as energias de interação de orbitais d_π calculados no nível de funcional de densidade para compostos modelo $[Pt(PH_3)_2(\eta^2\text{-}L)]$.

X-ray absorption spectra at the Pt $L_{2,3}$-edges have been measured for three $[Pt(PPh_3)_2(\eta^2\text{-}L)]$ {L = C_2H_4, C_{60} and $C_2(CN)_4$} compounds. The spectral features are effective for measuring the π^*-acid strength of ligands (L) coordinated to the $Pt(PPh_3)_2$ fragment. The energies of the d_π-orbitals are quantitatively determined using the difference between the edge jumping and the edge maximum shifts of the $L_{2,3}$-white lines in the second derivatives of the spectra. The d_π-orbital energies follow the order $[Pt(PPh_3)_2(\eta^2\text{-}C_2H_4)] < [Pt(PPh_3)_2(\eta^2\text{-}C_{60})] < [Pt(PPh_3)_2\{\eta^2\text{-}C_2(CN)_4\}]$. These d_π-orbital energies are in good agreement with the changes in the bound olefinic carbon bond lengths and the ^{31}P NMR chemical shifts of the coordinated phosphines. Furthermore, the experimental values are in good agreement with available d_π-orbital interaction energy terms calculated using density functional theory for model $[Pt(PH_3)_2(\eta^2\text{-}L)]$ compounds.

Keywords: Pt $L_{2,3}$-edge XAS, zerovalent platinum compounds, π back-donation energy, spectral decomposition

Introduction

X-ray absorption spectroscopy (XAS) is a powerful tool for characterising the electronic and structural properties of coordination complexes. Modern synchrotron radiation facilities make XAS an attractive experimental method for studying several absorbing transition metals.[1] XAS has the ability to probe both occupied and unoccupied 5d valence orbitals through studying the region of the Pt $L_{2,3}$ edges. Two absorption peaks (white lines) are observed at L_3- and L_2-edges and are split largely due to spin-orbit coupling. The $L_{2,3}$-edges identify the valence 5d-charges of the Pt center in accordance with the selection rules for the photoabsorption process ($\Delta l = \pm 1$ and $\Delta J = 0, \pm 1$). Because electrons are ejected from the 2p, $J = 3/2$, inner orbitals, the L_2 edge probes only the d-final orbitals that are characterised by $J = 3/2$, whereas the L_3 edge probes those d orbitals with $J = 3/2$ and 5/2. The allowed $2p \rightarrow 6s$ electric dipole transition is not observed because of the small spatial overlap between the 2p and the 6s wave functions.[2] For metals with a closed shell d^{10} configuration, the spectrum is a simple arctangent curve, which reflects the ejection of the electrons restricted to the core orbitals of the continuum Fermi-Sommerfeld levels.[3] A very nearly filled $5d_{3/2}$ state at the L_2 edge of Pt metal and its small clusters results in an insignificant d valence band contribution.[4] Consequently, the resultant spectrum can be also treated as an arctangent curve. In addition to metals with unoccupied 5d valence

*e-mail: herbst@ufrrj.br

orbitals, the valence-charge redistribution of a closed-shell d^{10}-metal upon alloy formation results in the emergence of prominent white lines at the L-edges. These absorptions provide useful signatures for d-charge depletions from the metal sites.[5] Therefore, these white lines are a key feature for interpreting the Pt $L_{2,3}$ XAS spectra of zerovalent platinum compounds.

Because the Pt L-edges directly probe the unoccupied 5d valence orbitals, assembling the correct information regarding the molecular orbitals would be useful, particularly considering that the coordination of side-on unsaturated ligands to a metal results in vacant d-orbitals on the metal center. The classical Dewar-Chatt-Duncanson model,[6] shown in Scheme 1, states that the occupied π orbitals on the ligands donate electron density to the unoccupied s- or d-orbitals (or sd-hybrids) of the metal (σ-donation) simultaneously with back-donation of electron density from occupied metal d orbitals to the empty π* orbital of the ligand (π back-donation). As a consequence, the carbon-carbon bond distance of the alkene ligand increases as a result of both decreased electron density in the bonding π-orbital and increased electron density in the antibonding π*-orbital.

Scheme 1. Ligand σ donation to metal ($a_1 \leftarrow \pi$) and metal to ligand π back-donation ($b_2 \rightarrow \pi^*$), according to the orbital interactions in the Dewar-Chatt-Duncanson model.

The compounds $[M(PH_3)_2(\eta^2\text{-}L)]$ {M = Ni, Pd, Pt; L = C_2H_4, C_{60}, $C_2(CN)_4$}, which are model compounds for $[Pt(PPh_3)_2(\eta^2\text{-}L)]$, have been the subject of study by several theoretical approaches.[7-9] The upper valence levels of the bent C_{2v} $Pt(PH_3)_2$ fragment have two available filled b_1 and b_2 platinum orbitals of d_π character. The π back-donation to the lowest unoccupied orbital (LUMO) of the ligand, which has π* character, mainly involves the highest occupied (HOMO) b_2 orbital. The HOMO lies in the PtC_2 plane, whereas the electron density donation from the filled HOMO π orbital of the ligand flows mainly into the 6s-6p_z platinum LUMO of a_1 symmetry (σ donation). Previous studies on $[Pt(PH_3)_2(\eta^2\text{-}L)]$ have identified that the major part of the covalent bonding energy term stems from π back-donation to the alkene ligand, which is particularly dependent on the position of the ligand π* energy level and the relativistic destabilisation of the Pt 5d valence orbitals.[9]

The rather unexpected experimental result of prominent white lines at $L_{2,3}$-edges within the structurally similar compounds $[Pt(PPh_3)_2(\eta^2\text{-}L)]$, shown in Scheme 2, allowed us to gain further insight into their chemistry.

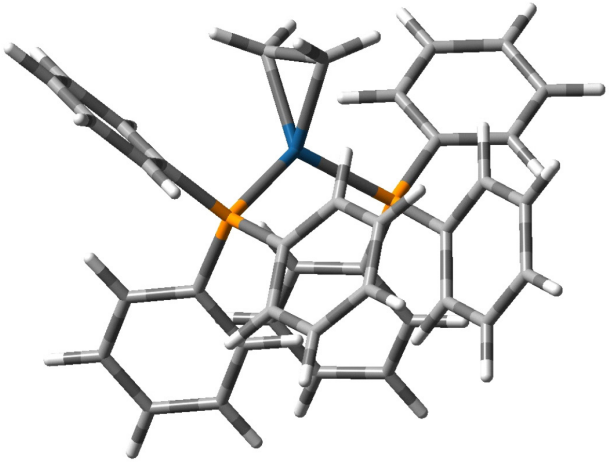

Scheme 2. Typical structure of the $[Pt(PPh_3)_2(\eta^2\text{-}L)]$ compounds, showing the crowd of triphenylphosphine ligands. Atom code: Pt (blue), P (orange), C (light gray), H (white).

We concentrate our study on the bond energy differences that result in the white lines in XAS spectra as a contribution to the development of a more efficient method in predicting the relative magnitude of the electronic density in such metal centers.[10] This method is based on the decomposition of the second derivative XAS spectra by using a rather simple model formed by an arctangent step function added to a Lorentzian function. Our results demonstrate that in analysing XAS spectra of organometallic compounds, in which electronic changes at the metal center are usually small, addressing only the absorption spectra is not sufficient; the second derivative provides a better means for accessing reliable data.

Results and Discussion

The white lines at the absorption edges are especially sensitive to the lifetime of the core holes as well as the localisation and hybridisation of the valence d orbitals. The absorption area, which stems from white lines, is often used for developing semi-quantitative estimations of the unoccupied levels of open d-shell metals. The usual method to obtain the area is by integrating the difference between the white lines and arctangent curves.[11] The arctangent background spectrum of a closed-shell d^{10}-metal, or a metal with an insignificant d valence band contribution to the white line, partially minimises the uncertainty that arises from the calibration using the EXAFS (extended X-ray absorption fine structure) oscillations. Another reliable

method for analysing XAS spectra is the decomposition of the white line into an absorption curve (usually a Lorentzian or a Voigt function) and an arctangent function, although this method can produce more than one result that matches the experimental data. In the refinement of nonlinear functions, white lines are fit to a combination of Lorentzian functions to model the absorption curve of the localised states and the remaining step-like arctangent function for the oscillatory components of the continuous states.[12] Thus, the decomposition method corresponds to the non-linear least-square fitting of the experimental data to a combination of a Lorentzian (or Voigt) and an arctangent functions. However, one must be aware that peak fitting is an empirical analysis method, and that the line shapes used to fit the experimental spectrum have little physical meaning. Thus, peak fitting should be used for semi-quantitative purposes, such as the relative variation of spectral features of similar compounds. Instrumental limitations, such as the thickness effect,[13] and the absence of a genuine arctangent function are other factors that can affect the results adversely in both methods. In this work we have used both the decomposition method and the subtraction of metallic gold XAS spectrum method. The decomposition method was best suited, concerning the fitting of the edge jumping (E_0) and the possibility of obtaining the fit of the second derivative of the spectra.

Figure 1 shows that the Pt L_3-XAS spectra of $[Pt(PPh_3)_2(\eta^2\text{-L})]$ compounds share similar features. Relatively strong and narrow white lines arise at the edge and are followed by deep EXAFS oscillations. In addition to the L_3 white line, a pronounced L_2 white line (not shown) was also observed, reflecting an unfilled $d_{3/2}$ characteristic for this edge. The proportional broadening of both edges was estimated by the L_3/L_2 area ratio, which reflects the contribution of the J = 3/2 and 5/2 hole populations.[14] This ratio is calculated by taking the integrated areas underneath the full Lorentzian peaks fit to the L_3 and L_2 edge spectra and dividing them in the form AL_3/AL_2. The values of AL_3 and AL_2 and of the area ratios are listed in Table 1. The area ratios are related to the d count in the sequence $[Pt(PPh_3)_2(\eta^2\text{-}C_2H_4)] < [Pt(PPh_3)_2(\eta^2\text{-}C_{60})] < [Pt(PPh_3)_2\{\eta^2\text{-}C_2(CN)_4\}]$ (Table 1). As a consequence of a large contribution of $d_{3/2}$ state to both edges, the L_3 edge was used in conjunction with L_2 to obtain more reliable values in the next stage.[15]

The spectral interpretation of the white lines, consistent with a quantitative description for the binding energy, was guided by the edge jumping energy (E_0), located in the inflection point at the rising edge, and the edge maximum (E_{max}) of the white line. For most typical complexes, it has been assumed that only the HOMO is involved at the

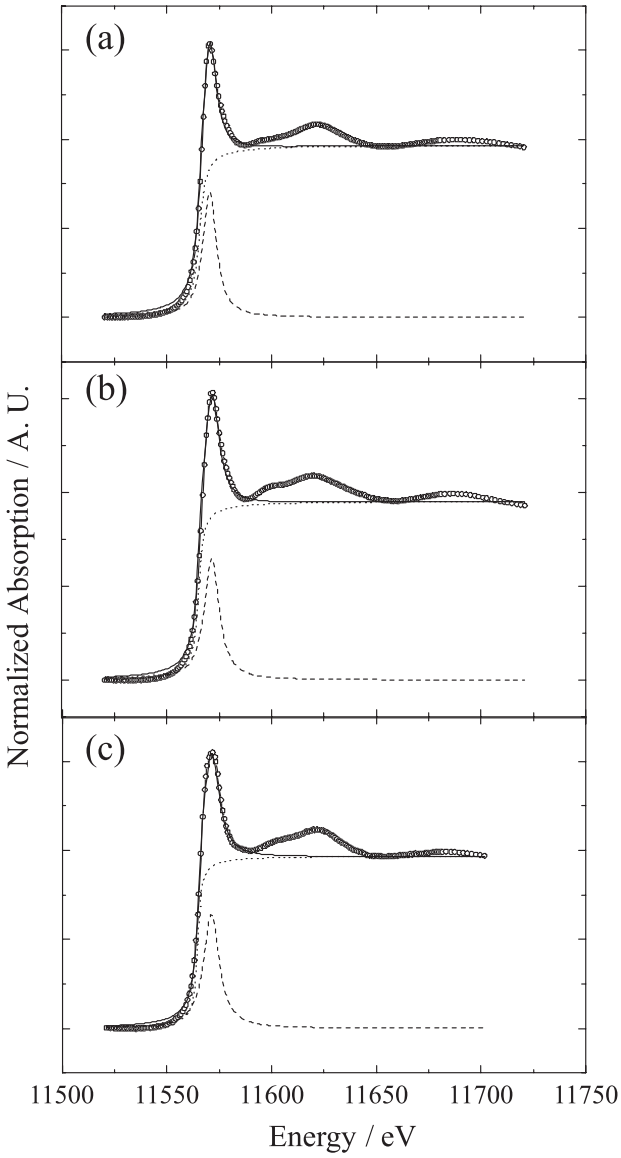

Figure 1. Experimental normalised Pt L_3-edge XAS absorption spectra of $[Pt(PPh_3)_2(\eta^2\text{-L})]$ compounds (small circles) plotted with the decomposed model spectra (solid line) and the model component curves (dashed line, Lorentzian curve; dotted line, arctangent curve). (a) $[Pt(PPh_3)_2(\eta^2\text{-}C_2H_4)]$, (b) $[Pt(PPh_3)_2(\eta^2\text{-}C_{60})]$ and (c) $[Pt(PPh_3)_2\{\eta^2\text{-}C_2(CN)_4\}]$.

E_0, whereas the E_{max} reflects the LUMO holes in an MO description.[16] Moreover, the E_{max} shifts to a higher energy concomitantly with the white line broadening. As a result, the difference between E_{max} and E_0 has an approximate value of the half-width of the raising edge.[17] The HOMO is naturally located in the E_0 for the particular case of $[Pt(PR_3)_2L]$ compounds, while the E_{max} reflects the holes created mainly on the b_2-hybrid orbital by back-bonding into the relatively localised LUMO. Therefore, the $\Delta E_\pi = E_{max} - E_0$ can be related to the d_π-orbital interaction energy. The main edge feature of $[Pt(PPh_3)_2(\eta^2\text{-L})]$ compounds is the broadening of the white-line in the XAS spectra (Figure 1), which is more

Table 1. Selected results of the Pt $L_{2,3}$-edges XAS and the relevant ancillary data for $[Pt(PPh_3)_2(\eta^2\text{-}L)]$ {L = C_2H_4, C_{60}, $C_2(CN)_4$}

Compound	AL_3 [a]	AL_2 [a]	R [b]	ΔE_π L_3	ΔE_π L_2	ΔE_π [c]	ΔE_t [d]	ΔR [e]	ΔP [f]
$[Pt(PPh_3)_2(\eta^2\text{-}C_2H_4)]$	8.28	4.61	1.8	3.5	3.3	3.40	3.19	0.095	39.6
$[Pt(PPh_3)_2(\eta^2\text{-}C_{60})]$	8.42	3.81	2.2	4.9	4.8	4.85	4.60	0.119	31.8
$[Pt(PPh_3)_2(\eta^2\text{-}C_2(CN)_4)]$	8.72	3.47	2.5	6.7	6.3	6.50	5.81	0.180	20.9

[a]Areas at L_3 (mean ± 0.2) and L_2 (mean ± 0.4) edges in eV *per* cm^2. [b]Area ratio AL_3/AL_2. [c]Average $L_{2,3}$ edges energy $\Delta E_\pi = E_{max} - E_0$ (mean ± 0.03) in eV. [d]Sum $\Delta E_t = E_{B2} + E_{B1}$ in eV from Nunzi *et al.*[8] [e]Elongation parameter ΔR. Difference between the carbon-carbon bond lengths of coordinated and free molecules in angstroms. [f]Difference between the chemical shifts of ^{31}P coordinated and ^{31}P of free PPh_3 in ppm.

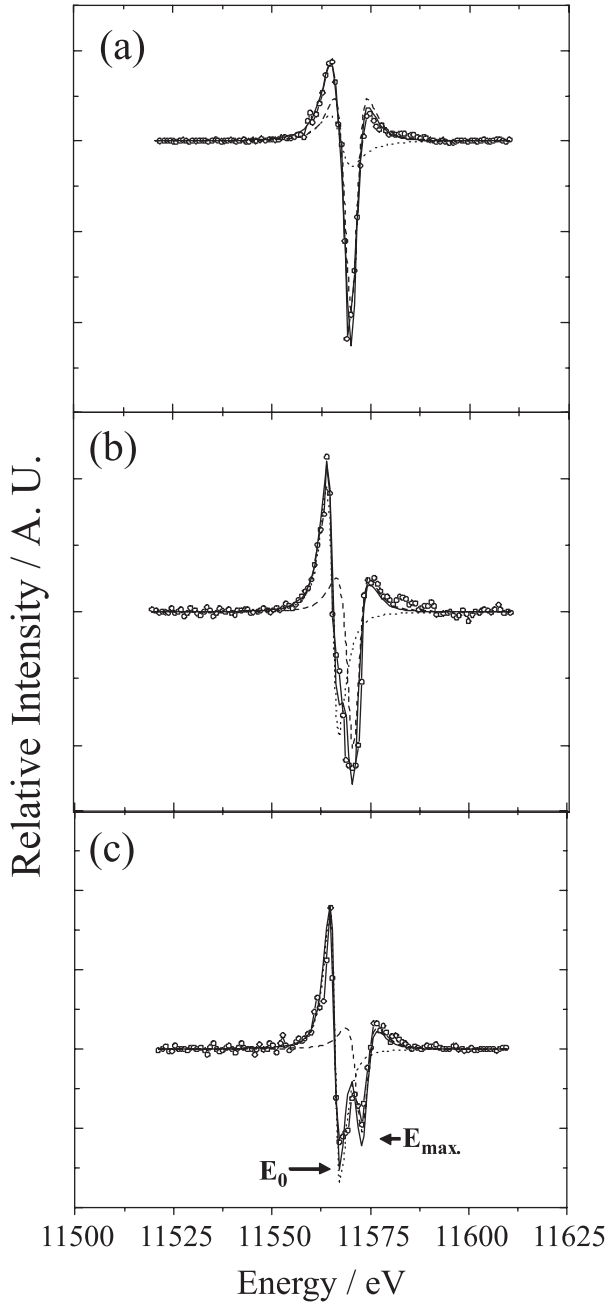

Figure 2. Second derivatives of the normalised Pt L_3-edge XAS spectra of $[Pt(PPh_3)_2(\eta^2\text{-}L)]$ compounds (small circles) plotted with the decomposed second derivatives spectra (solid line). The symbols for lorentzian and arctangent curves are the same of those in Figure 1. (a) $[Pt(PPh_3)_2(\eta^2\text{-}C_2H_4)]$, (b) $[Pt(PPh_3)_2(\eta^2\text{-}C_{60})]$ and (c) $[Pt(PPh_3)_2\{\eta^2\text{-}C_2(CN)_4\}]$.

distinguishable as a doublet growth in the second derivative spectra shown in Figure 2.

The splitting observed in the second derivative of the XAS spectrum is influenced by the degree of vacancy in 5d levels. With regard to this spectral pattern, the experimental and deconvoluted second derivatives were used as guides in determining the energy positions of peaks more accurately.[18] Table 1 presents selected results for the Pt $L_{2,3}$-edges XAS and relevant ancillary data for the $[Pt(PPh_3)_2(\eta^2\text{-}L)]$ compounds.

The energy values listed in Table 1 are as expected, where ΔE_π is related to both the elongation parameter (ΔR) and the coordination chemical shift (ΔP), calculated from literature data for free and coordinated ligands listed in Table 2.

Table 2. Collected literature data for free and coordinated ligands

Molecule	C-C bond distance / Å	δ ^{31}P NMR / ppm	Reference
C_2H_4	1.339(5)	-	19
C_{60}	1.383(4)	-	20
$C_2(CN)_4$	1.67	-	21
PPh_3	-	–5.6	22
$[Pt(PPh_3)_2(\eta^2\text{-}C_2H_4)]$ (**1**)	1.434(13)	34.0 (CD_2Cl_2)	23
$[Pt(PPh_3)_2(\eta^2\text{-}C_{60})]$ (**2**)	1.502(30)	26.2 (CD_2Cl_2)	28
$[Pt(PPh_3)_2\{\eta^2\text{-}C_2(CN)_4\}]$ (**3**)	1.49(5)	26.2 (CD_2Cl_2)	24

In Figure 3, significant trends are observed. The plot of ΔE_π against ΔR follows the usual order $[Pt(PPh_3)_2(\eta^2\text{-}C_2H_4)] < [Pt(PPh_3)_2(\eta^2\text{-}C_{60})] < [Pt(PPh_3)_2\{\eta^2\text{-}C_2(CN)_4\}]$, which can be explained by the strength of the d_π back-donation interaction.

The progressive destabilisation of the b_2-type d_π donor orbital level, as the energy level of the olefin LUMO in $Pt(PPh_3)_2$ moiety decreases, will decrease the $d_\pi - \pi^*$ energy gap. Because ΔP is inversely proportional to ΔE_π, the ^{31}P chemical shift of the bonded PPh_3, which is upfield relative to the free molecule, indicates that the energy of the HOMO b_2 orbital increases. This fact is expected in view of the σ-donor properties of the lone pair orbital on the ancillary PPh_3 ligands, which mixes in an antibonding manner with

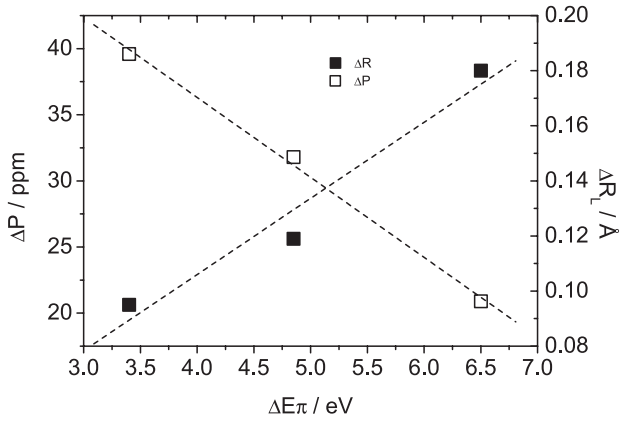

Figure 3. Plot of the energy, ΔE_π, *versus* ΔP and ΔR. Experimental uncertainties in bond distances are in the 0.01 Å range, in ^{31}P chemical shifts are 0.1 ppm, following the original reports. Uncertainties in ΔE_π are 0.03 eV. The dashed lines indicate the trend in the data.

the antisymmetric b_2 combination. The predicted amount of charge withdrawn from the $Pt(PPh_3)_2$ fragment by back-donation is greater for the tetracyanoethylene ligand in $[Pt(PPh_3)_2(\eta^2\text{-L})]$ complexes. The ethylene ligand removes approximately half the amount of tetracyanoethylene, whereas fullerene-60 withdraws an intermediate amount.

It is noteworthy that the XAS data are in good agreement with the results of a density functional theory calculation that has been performed on model complexes.[25] Theoretical procedures decompose part of the total binding energy of $[(PH_3)_2Pt(\eta^2\text{-L})]$ complexes into the orbital interaction term energy $E_{orb} = E_{A1} + E_{B2} + E_{B1}$. The energy contributions from the two synergistic bonding modes originate from stabilising interactions between occupied and virtual orbitals of separate $(PH_3)_2Pt$ and L fragments, corresponding to σ donation (E_{A1}) and to π back-donation ($\Delta E_t = E_{B2} + E_{B1}$).[26] The theoretical contribution of the sum of the d-hybrid orbitals, which are depopulated upon coordination, ΔE_t, was plotted against the experimental ΔE_π in Figure 4.

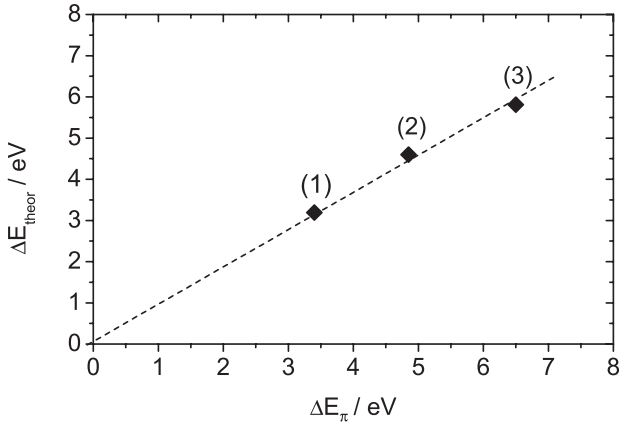

Figure 4. The relationship between ΔE_π and ΔE_{theor}. Extrapolation of the line to the zero intercept indicates the trend in the data.

The convergence of the resulting line and the hypothetical zero point energy suggests that this point would fall in the line. Because PH_3 is used as model for PPh_3 in the ΔE_t calculation, the π-acceptor properties of the phosphine ligand are neglected. Energy values between the experimental ΔE_π and the theoretical ΔE_t, which are smaller than 1 eV in Table 1, can be related to back-donation to the d orbital of the phosphorus atom.

Experimental

Preparation of complexes

The $[Pt(PPh_3)_2(\eta^2\text{-}C_2H_4)]$ (**1**),[27] $[Pt(PPh_3)_2(\eta^2\text{-}C_{60})]$ (**2**)[28] and $[Pt(PPh_3)_2\{\eta^2\text{-}C_2(CN)_4\}]$ (**3**)[29] complexes were synthesised as described elsewhere and stored under argon prior to use.

X-ray absorption spectroscopy measurements and data analysis

The experimental spectra at the Pt $L_{2,3}$ edges were recorded at the National Synchrotron Light Laboratory (LNLS, Campinas, SP, Brazil), using the synchrotron radiation at an energy of 1.37 GeV with an average ring current of 120 mA. The Pt $L_{2,3}$-edge XAS spectra were measured on the XAFS I station equipped with a double crystal Si(220) monochromator in transmission mode and two silicon crystals that were slightly detuned to avoid higher harmonics. The XAS data were collected with a 1s accumulation time per point and an energy increment of 0.5 eV in transmission mode at room temperature by using two ionisation chambers filled with argon and measuring the incident (monitor) and transmitted (detector) beam intensity. The powder samples were pasted on a grid carved on a lead metal sheet and capped with Kapton tape. The spectrum of a 7.5 μm platinum metal foil was recorded before and after each XAS spectrum to check energy calibration. All spectra were normalised to unity in the continuum absorption across the absorption edges, such that the step heights coincide.

Conclusions

Pt $L_{2,3}$ XAS proved to be a powerful quantitative tool for probing the energy of vacant d-orbitals in the triad of compounds $[Pt(PPh_3)_2(\eta^2\text{-L})]$ {L = C_2H_4, C_{60}, $C_2(CN)_4$}, determining the d_π-orbital interaction energy term and reinforcing the underlying concepts of the Dewar-Chatt-Duncanson model. The charge withdrawn in terms of energy from the $Pt(PPh_3)_2$ fragments to the alkene

ligands increases in the order $[Pt(PPh_3)_2(\eta^2\text{-}C_2H_4)]$ < $[Pt(PPh_3)_2(\eta^2\text{-}C_{60})]$ < $[Pt(PPh_3)_2(\eta^2\text{-}C_2(CN)_4)]$. It is important to note that for obtaining reliable data from the XAS spectra of organometallic compounds, it is more appropriate to employ the second derivative spectral decomposition than the absorption spectrum itself, due to the usually small changes in electronic density upon complex formation. Finally, the XAS data act as a good reference for the density functional theory data, showing that the differences in the entire binding energy resulting from the approximation of PPh_3 with PH_3 are not negligible.

Acknowledgments

We thank the Fundação de Amparo à Pesquisa do Estado de São Paulo (FAPESP) for support of this research (grant 97/11567-7). This work was also partially supported by LNLS. Authors are grateful to an anonymous referee for valuable suggestions.

References

1. Bianconi, A.; Garcia, J.; Benfatto, M.; *Top. Curr. Chem.* **1988**, *145*, 29; Bianconi, A. In *X-Ray Absorption: Principles, Applications, Techniques of EXAFS, SEXAFS and XANES*; Koningsberger, D. C.; Prins, R., eds.; Wiley: New York, 1988; Penner-Hahn, J. E.; *Coord. Chem. Rev*. **1999**, *192*, 1101.
2. Pantelouris, A.; Küper, G.; Hormes, J.; Feldmann, C.; Jansen, M.; *J. Am. Chem. Soc*. **1995**, *117,* 11749; Brown, M.; Peierls, R. E.; Stern, E. A.; *Phys. Rev. B: Condens. Matter Mater. Phys.* **1977**, *15*, 738; Hitchcock, A. P.; Wen, A. T.; Rühl, E.; *Chem. Phys*. **1990**, *147*, 51.
3. Richtmyer, F. K.; Barnes, S. W.; Ramberg, E.; *Phys. Rev.* **1934**, *46*, 843.
4. Ramaker, D. E.; Mojet, B. L.; Oostenbrink, M. T. G.; Miller, J. T.; Koningsberger, D. C.; *Phys. Chem. Chem. Phys.* **1999**, *1*, 2293.
5. Behrens, P.; Assmann, S.; Bilow, U.; Linke, C.; Jansen, M.; *Z. Anorg. Allg. Chem*. **1999**, *625*, 111; Behrens, P.; *Solid State Commun*. **1992**, *81*, 235; Naftel, S. J.; Bzowski, A.; Sham, T. K.; *J. Alloys Compd.* **1999**, *283*, 5; Drube, W.; Treusch, R.; Sham, T. K.; Bzowski, A.; Soldatov, A. V.; *Phys. Rev. B: Condens. Matter Mater. Phys.* **1998**, *58*, 6871; Jeon, Y.; Qi, B. Y.; Lu, F.; Croft, M.; *Phys. Rev. B: Condens. Matter Mater. Phys.* **1989**, *40*, 1538.
6. Dewar, M. J. S.; *Bull. Soc. Chim. Fr*. **1951**, *18*, C79; Chatt, J.; Duncanson, L. A.; *J. Chem. Soc*. **1953**, 2939.
7. Albright, T. A.; Hoffmann, R.; Thibeault, J. C.; Thorn, D. L.; *J. Am. Chem. Soc*. **1979**, *101*, 3801; Ziegler, T.; *Inorg. Chem.* **1985**, *24*, 1547; Morokuma, K.; Borden, W. T.; *J. Am. Chem. Soc*. **1991**, *113*, 1912; Nunzi, F.; Sgamellotti, A.; Re, N.; Floriani, C.; *J. Chem. Soc., Dalton Trans*. **1999**, 3487; Uddin, J.; Dapprich, S.; Frenking, G.; Yates, B. F.; *Organometallics* **1999**, *18*, 457.
8. Fujimoto, H.; Nakao, Y.; Fukui, K.; *J. Mol. Struct*. **1993**, *300*, 425; Koga, N.; Morokuma, K.; *Chem. Phys. Lett*. **1993**, *202*, 330; Lichtenberger, D. L.; Wright, L. L.; Gruhn, N. E.; Rempe, M. E.; *J. Organomet. Chem*. **1994**, *478*, 213; López, J. A.; Mealli, C.; *J. Organomet. Chem*. **1994**, *478*, 161; Nunzi, F.; Sgamellotti, A.; Re, N.; Floriani, C.; *Organometallics* **2000**, *19*, 1628; Craciun, R.; Vincent, A. J.; Shaughnessy, K. H.; Dixon, D. A.; *Inorg. Chem*. **2010**, *49*, 5546.
9. Li, J.; Schreckenbach, G.; Ziegler, T.; *Inorg. Chem*. **1995**, *34*, 3245.
10. C_{60} is herein treated as an electron-deficient polyalkene.
11. Jeon, Y.; Chen, J.; Croft, M.; *Phys. Rev. B: Condens. Matter Mater. Phys.* **1994**, *50*, 6555; Benfield, R. E.; Grandjean, D.; Kröll, M.; Pugin, R.; Sawitowski, T.; Schmid, G.; *J. Phys. Chem. B* **2001**, *105*, 1961.
12. Outka, D. A.; Stöhr, J.; *J. Chem. Phys*. **1988**, *88*, 3539; Mansour, A. N.; Cook Jr., J. W.; Sayers, D. E.; *J. Phys. Chem*. **1984**, *88*, 2330.
13. Choy, J. -H.; Kim, D. -K.; Demazeau, G.; Jung, D. -Y.; *J. Phys. Chem*. **1994**, *98*, 6258.
14. Pease, D. M.; Fasihuddin, A.; Daniel, M.; Budnick, J. I.; *Ultramicroscopy* **2001**, *88*, 1.
15. Sham, T. K.; *Phys. Rev. B: Condens. Matter Mater. Phys.* **1985**, *31*, 1888; Sham, T. K.; *Solid State Commun*. **1987**, *64*, 1103; de Groot, F. M. F.; Hu, Z. W.; Lopez, M. F.; Kaindl, G.; Guillot, F.; Tronc, M.; *J. Chem. Phys.* **1994**, *101*, 6570.
16. Qi, B.; Perez, I.; Ansari, P. H.; Lu, F.; Croft, M.; *Phys. Rev. B: Condens. Matter Mater. Phys.* **1987**, *36*, 2972.
17. Sham, T. K.; *Phys. Rev. B: Condens. Matter Mater. Phys.* **1985**, *31*, 1903.
18. Lytle, F. W.; Greegor, R. B.; *Appl. Phys. Lett*. **1990**, *56*, 192; Wang, W. -C.; Chen, Y.; Hu, T. -D.; *Phys. Status Solidi B* **1994**, *186*, 545.
19. Costain, C. C.; Stoicheff, B. P.; *J. Chem. Phys*. **1959**, *30*, 777.
20. Fedurco, M.; Olmstead, M. M.; Fawcett, W. R.; *Inorg. Chem*. **1995**, *34*, 390.
21. Bekoe, D. A.; Trueblood, K. N.; *Z. Kristallogr*.**1960**, *113*, 1.
22. Asaro, F.; Lenarda, M.; Pellizer, G.; Storaro, L.; *Spectrochim. Acta, Part A* **2000**, *56*, 2167; Pellizer, G.; Graziani, M.; Lenarda, M.; *Polyhedron* **1983**, *2*, 657; Berger, S.; Braun, S.; Kalinnowski, H. -O.; *NMR Spectroscopy of the Non-Metallic Elements*; Wiley: Chichester, 1977, p. 709.
23. Cheng, P. -T.; Nyburg, S. C.; *Can. J. Chem*. **1972**, *50*, 912.
24. Bombieri, G.; Forselli, E.; Panattoni, C.; Graziani, R.; Bandoli, G.; *J. Chem. Soc. A* **1970**, 1313.
25. Karhánek, D.; Kacer, P.; Kuzma, M.; Splíchalová, J.; Cervený, L.; *J. Mol. Model*. **2007**, *13*, 1009.

26. Frenking, G.; Fröhlich, N.; *Chem. Rev*. **2000**, *100*, 717 and references therein.
27. Nagel, U.; *Chem. Ber*. **1982**, *115*, 1998.
28. Fagan, P. J.; Calabrese, J. C.; Malone, B.; *Science* **1991**, *252*, 1160.
29. Baddley, W. H.; Venanzi, L. M.; *Inorg. Chem*. **1966**, *5*, 33.

Submitted: January 25, 2011
Published online: October 13, 2011

FAPESP has sponsored the publication of this article.